CHAPTER 4

THEORETICAL AND EXPERIMENTAL STUDIES OF PYRANOPYRAZOLES AND THEIR TRIBOLOGICAL COMPATIBILITY WITH A BORATE ESTER

The perpetual search for newer compounds in this category is imperative for the development of better and better antiwear and antifriction additives. Motivated by our results of tetrahydropyrazopyridines (a fused ring system of pyrazoles and pyridine) shown in the previous chapter, another fused heterocyclic ring system of pyrazole with pyran, substituted pyranopyrazoles (PPz-R, R = H, Me, OMe) was contemplated for high tribological efficacy. Accordingly, substituted pyranopyrazoles were synthesized via a multicomponent reaction between hydrazine hydrate, ethyl acetoacetate, malononitrile, and the corresponding aldehyde [Vasuki et al. (2008), Nagarajan et al. (2009), Kiyani et al. (2013)]. The tribological activities of these substituted pyranopyrazoles in paraffin oil (PO) with ZDDP as a reference additive were investigated using a four-ball tester. Quantum chemical calculations using Density Functional Theory (DFT) were also performed to validate the experimentally observed data. The antiwear properties of additives to lubricants depend critically on their adsorption to the surface material [Ta et al. (2015)]. Hence, the mechanism of adsorption of pyranopyrazole derivatives in paraffin on an iron slab was studied using molecular dynamics (MD) simulations. The emphasis was on the details of molecular interaction between additive molecule parts and the adsorbent atoms. These aspects were elucidated through radial distribution function (RDF) and adsorption energy calculations.

Environment-friendly oil-soluble organic borate esters with high hydrolytic stability have been reported as excellent antiwear additives [Li.et al. (2010)]. Some N-containing heterocyclic borate esters have shown improved tribological performance involving intramolecular coordination between electron-rich nitrogen and electron- deficient boron [He et al.(2018)]. This kind of synergism has also been exhibited between antipyrine Schiff bases

and borate esters [Jaiswal et al.(2014)] from our laboratory. For the furtherance of the tribological activity of pyranopyrazoles, the admixture of the best additive, PPz-OMe, was prepared with borate ester (Van lube) in paraffin oil (PO) and tested on a four-ball tester for the tribo- activity.

4.1. Experimental section

4.1.1. Chemicals

The analytical grade chemicals like hydrazine hydrate, ethyl acetoacetate, benzaldehyde, *p*-methyl- and *p*-methoxy benzaldehydes, malononitrile, ethanol, ethyl acetate, and n-hexane used throughout the investigation were procured from Merck, India. Paraffin oil was obtained from Qualigens Fine Chemicals. Van lube 289, containing borate ester as the main component, was obtained as a gift material. This is a yellow liquid (color ASTM D1500 L1.5) with boron content 1.00 %, density 0.99 mg mm^{-3} at 15.6 ^{o}C and viscosity 458.00 cSt and 22.30 cSt at 40 ^{o}C and 100 ^{o}C, respectively.

4.1.2. Synthesis of pyranopyrazole derivatives

For a typical synthesis of pyranopyrazole [Vasuki et al. (2008)], hydrazine hydrate (5 mmol) and ethyl acetoacetate (5 mmol) were taken together in a round bottom flask and stirred continuously until the mixture solidified at room temperature. The resulting solid, 3- methyl-5-pyrazolone, was dissolved in 20 ml of ethanol, an aromatic aldehyde (5mmol) and malononitrile (5mmol) were added successively, and the reaction mixture was refluxed for 3 h. Thin-layer chromatography applying ethyl acetate and n-hexane in 30:70 ratios was used to see the progress of the reaction. The final product was filtered and washed with a mixture of ethyl acetate and n-hexane (20:80), followed by ethanol **(Fig 4.1)**. The final product was further

purified by recrystallization with ethanol and characterized by FTIR and NMR (^{1}H and ^{13}C) spectroscopic techniques. The FTIR, ^{1}H NMR, and ^{13}C NMR spectra of the synthesized additives are shown in **Figs. 4.2-4.8**. The IUPAC names, abbreviations, structures, and characterization of the pyranopyrazole are given in **(Table 4.1)**.

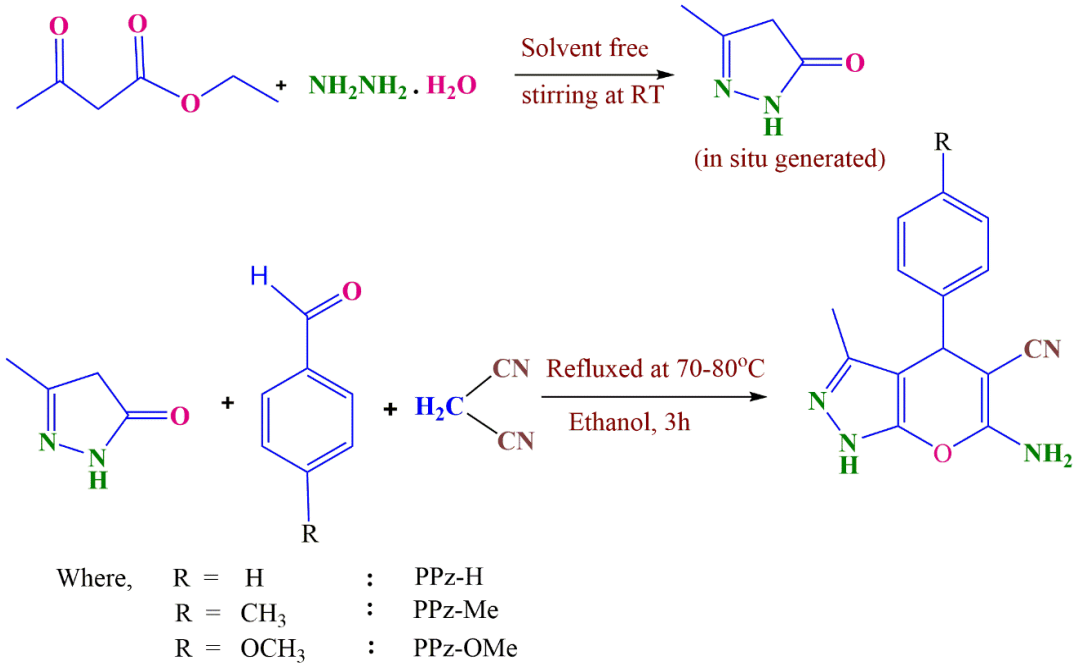

Fig. 4.1. Synthesis of pyranopyrazoles using substituted aldehydes

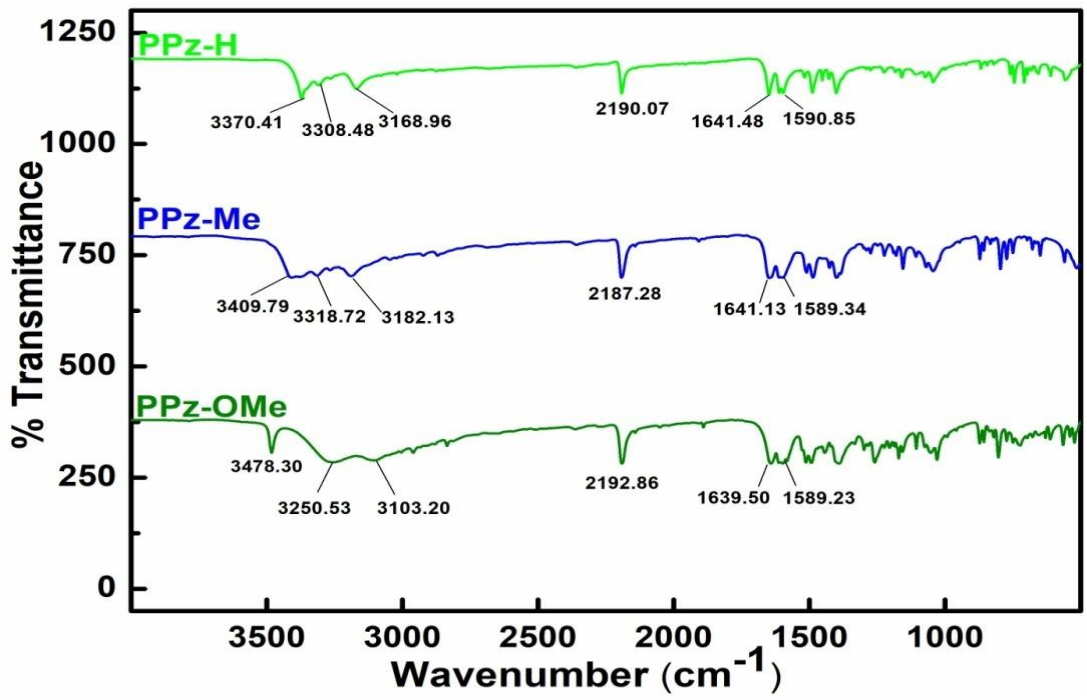

Fig. 4.2. IR Spectrum of different pyranopyrazole additives

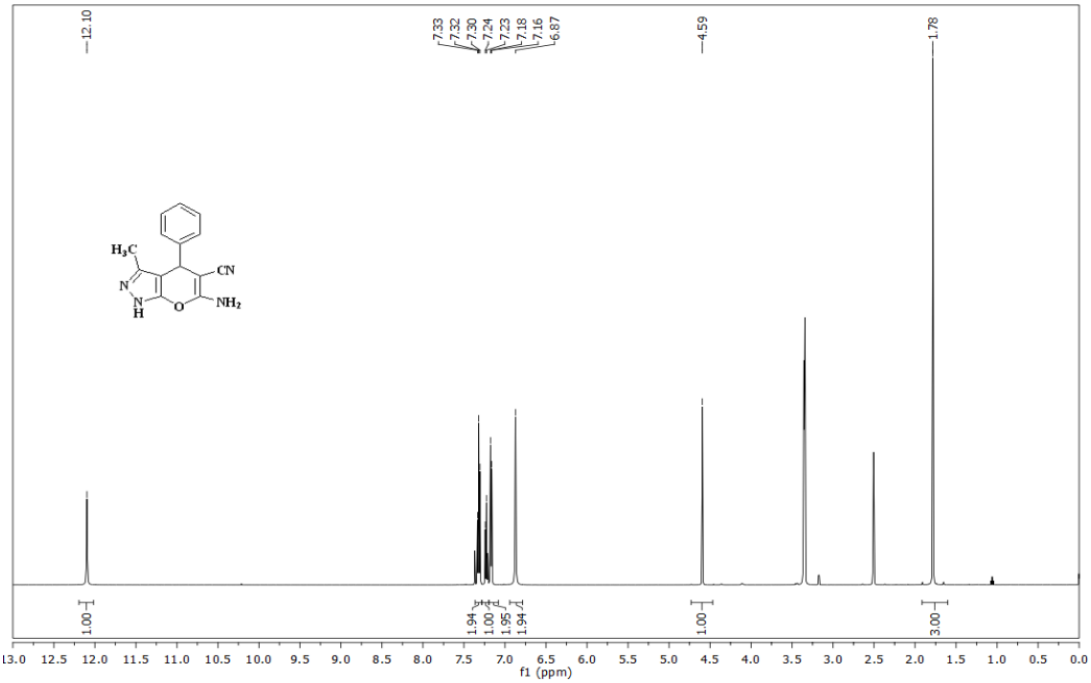

Fig. 4.3. ^{1}H NMR Spectrum of PPz-H

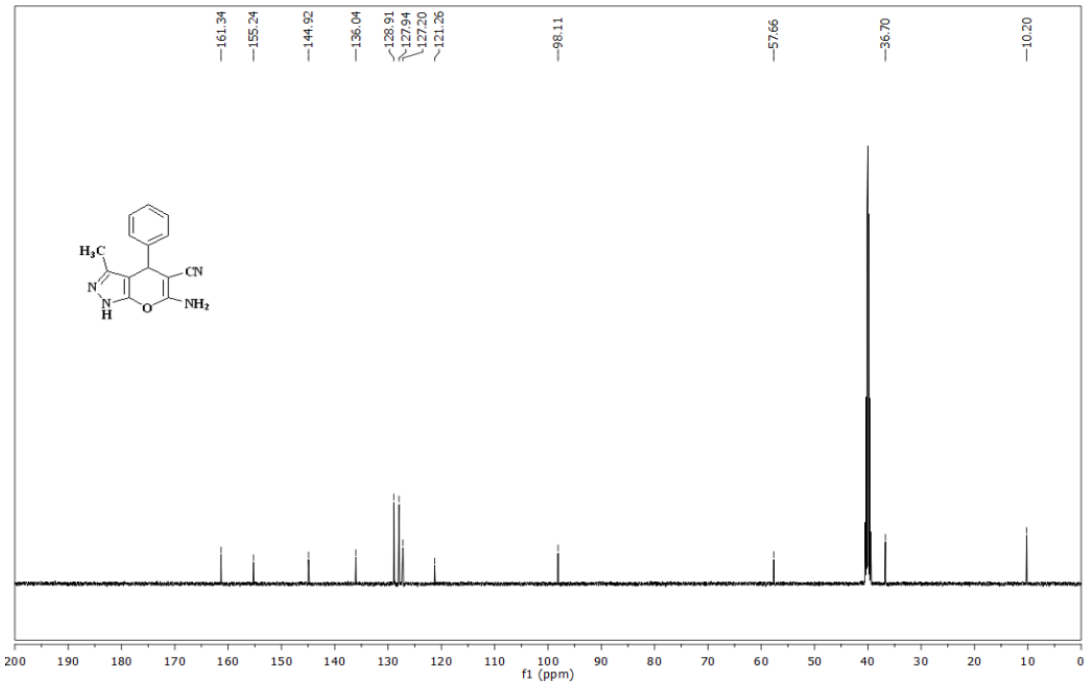

Fig. 4.4. ^{13}C NMR Spectrum of PPz-H

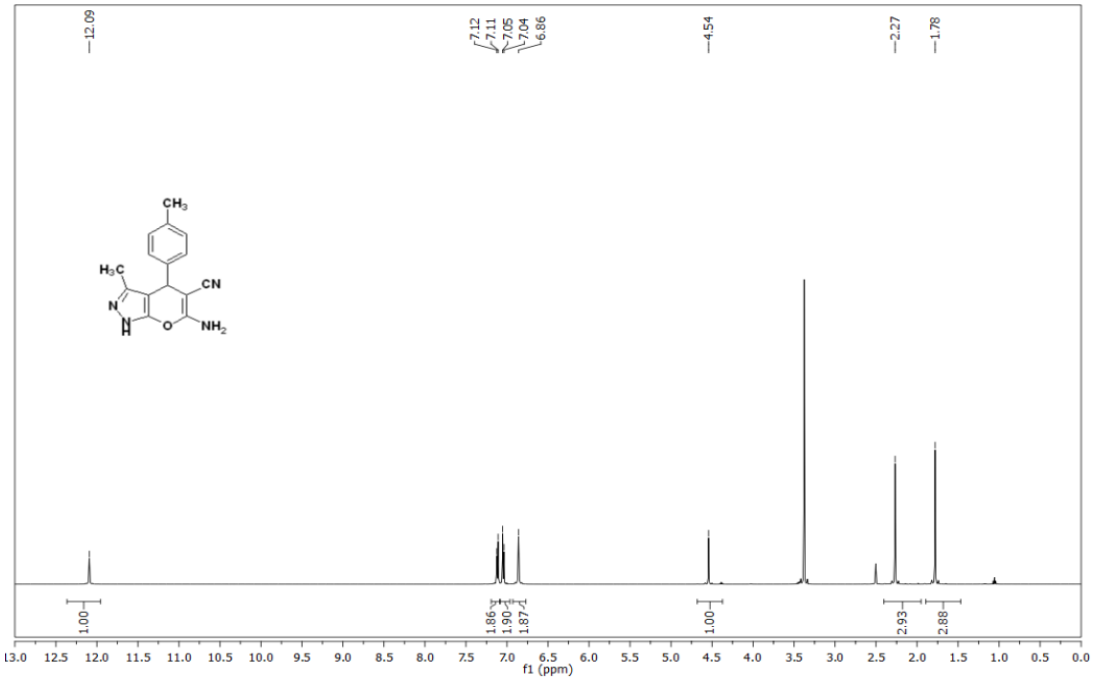

Fig. 4.5. ^{1}H NMR Spectrum of PPz-Me

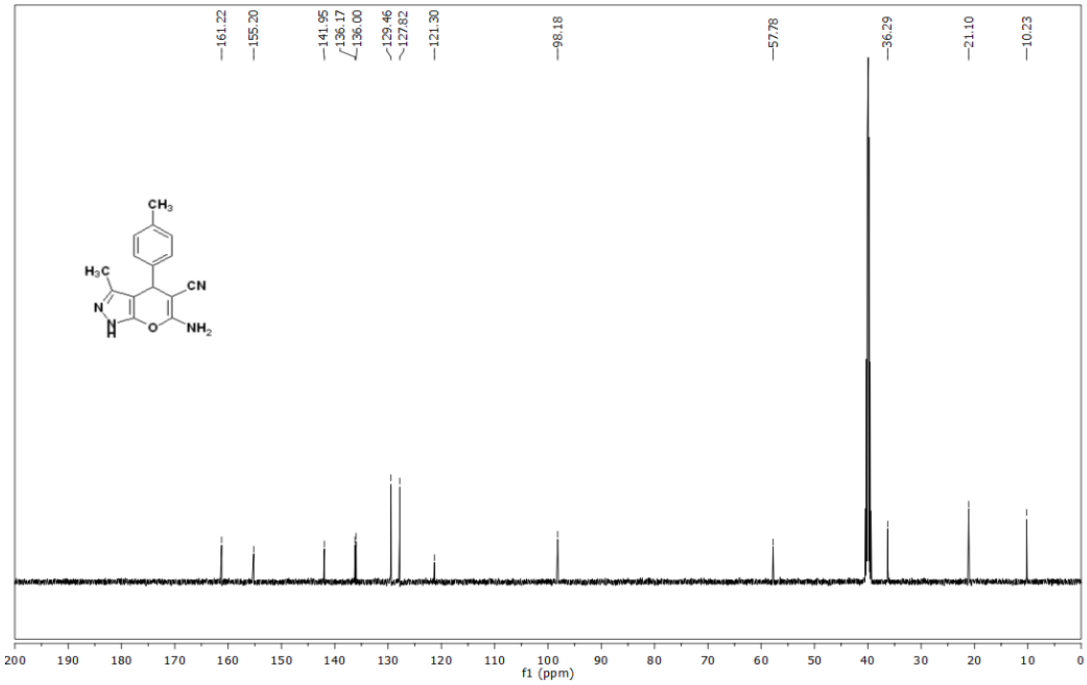

Fig. 4.6. ^{13}C NMR Spectrum of PPz-Me

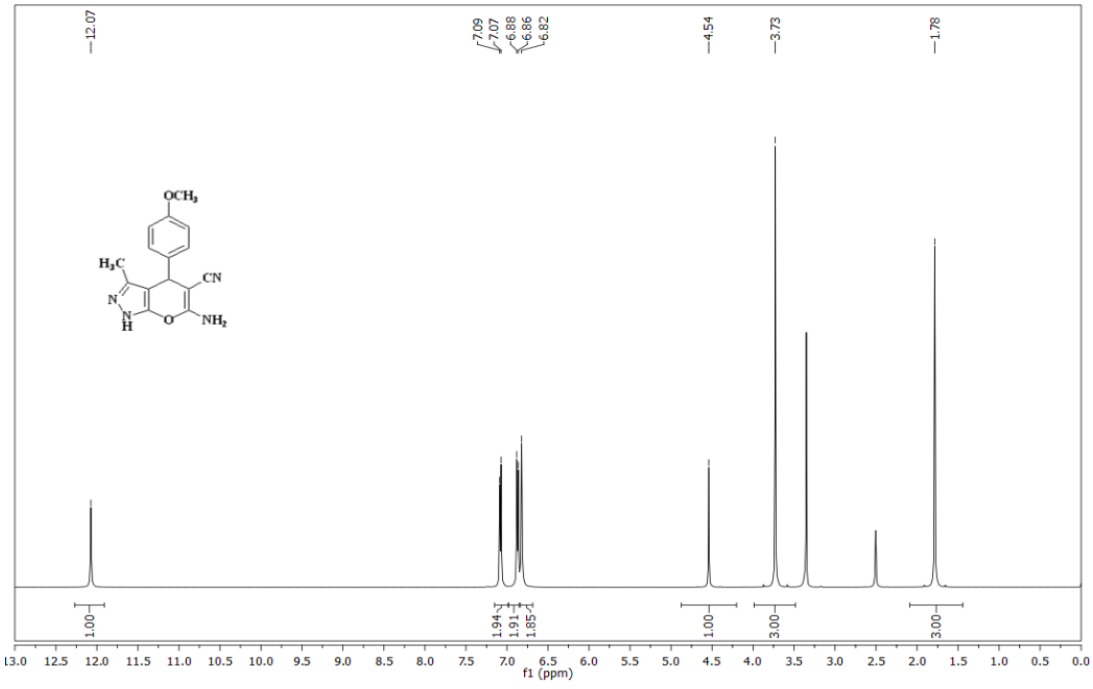

Fig. 4.7. ^{1}H NMR Spectrum of PPz-OMe

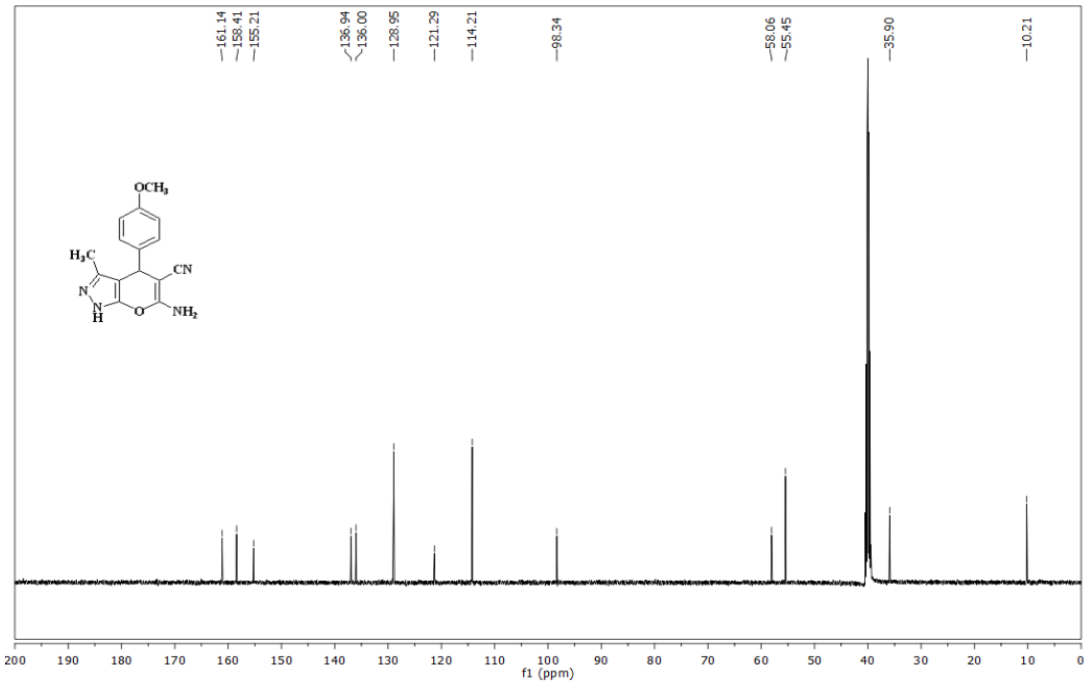

Fig. 4.8. ^{13}C NMR Spectrum of PPz-OMe

Table 4.1 Molecular structures, IUPAC names**,** abbreviations, and characterizations of the pyranopyrazole derivatives (PPz-H, PPz-Me, PPz-OMe)

S.N.	Structure	IUPAC name and abbreviation	Characterization
1	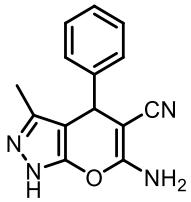	6-amino-3-methyl-4-phenyl-1,4-dihydropyrano[2,3-c]pyrazole-5-carbonitrile (PPz-H)	M.P. : 242°C, white solid FTIR(KBr,cm^{-1}): ν_{max} = 3370.41 (NH), 3308.48 and 3168.96 (NH_2), 2190.07 (CN), 1641.48 (C=N), 1590.85 (C=C); ^{1}H NMR (500 MHz, DMSO-d_6) δ 12.10(s, 1H), 7.33-7.30 (t, 2H), 7.24 – 7.23 (d, 1H), 7.18-7.16 (d, 2H), 6.87 (s, 2H), 4.59 (s, 1H), 1.78 (s, 3H). ^{13}C NMR (126 MHz, DMSO-d_6) δ 161.34, 155.24, 144.92, 136.04, 128.91, 127.94, 127.20, 121.26, 98.11, 57.66, 36.70, 10.20.
2	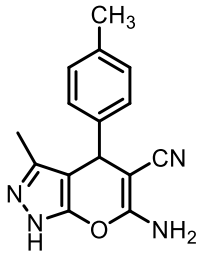	6-amino-3-methyl-4-(4-methylphenyl)-1,4-dihydropyrano[2,3-c]pyrazole-5-carbonitrile (PPz-Me)	M.P. : 194°C, white solid FTIR(KBr,cm^{-1}): ν_{max} = 3409.79 (NH) , 3318.72 and 3182.13 (NH_2), 2187.28 (CN), 1641.13 (C=N), 1589.34 (C=C); ^{1}H NMR (500 MHz, DMSO-d_6) δ 12.09(s, 1H), 7.12-7.11 (d, 2H), 7.05-7.04 (d, 2H), 6.86 (s, 2H), 4.54 (s, 1H), 2.27 (s, 3H), 1.78 (s, 3H). ^{13}C NMR (126 MHz, DMSO-d_6) δ 161.22, 155.20, 141.95, 136.17, 136.00, 129.46, 127.82, 121.30, 98.18, 57.78, 36.29, 21.10, 10.23.
3	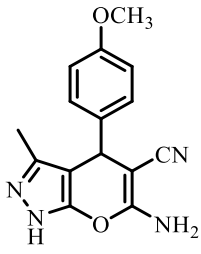	6-amino-3-methyl-4-(4-methoxyphenyl)-1,4-dihydropyrano[2,3-c]pyrazole-5-carbonitrile (PPz-OMe)	M.P. : 210°C, yellow solid FTIR(KBr,cm^{-1}): ν_{max}= 3478.30 (NH) , 3250.53 and 3103.20 (NH_2), 2192.86 (CN), 1639.50 (C=N), 1589.23 (C=C); ^{1}H NMR (500 MHz, DMSO-d_6) δ 12.07 (s, 1H), 7.09-7.07 (d, 2H) , 6.88-6.86 (d, 2H), 6.82 (s, 2H), 4.54 (s, 1H), 3.73 (s, 3H), 1.78 (s, 3H). ^{13}C NMR (126 MHz, DMSO-d_6) δ 161.14, 158.41, 155.21, 136.94, 136.00, 128.95, 121.29, 114.21, 98.34, 58.06, 55.45, 35.90, 10.21.

4.1.3. Tribological behavior

Uniform dispersions of pyranopyrazoles in paraffin oil (0.00, 0.125, 0.25, 0.50, 0.75, and 1.00 % w/v) were prepared by 1h sonication. The optimized concentration of the additives was used further for tribological tests.

4.1.4. Computational details for DFT and molecular dynamics simulations studies

Density Functional Theory (DFT) calculations were carried out by B3LYP. Full geometry optimizations of all additives were conducted with the standard B3LYP/6-31G + (d, p) basis set using Gaussian 03, revision C. 01 [Dapprich et al. (2004)].

The Scienomics software Materials and Process Simulation (MAPS) version 4.01 was used to make the input models for the MD simulations [Sarl et al. (2014)]. Three separate models were constructed. The first step was the construction of the initial structures of three pyranopyrazole derivatives named PPz-H, PPz-Me, and PPz-OMe for the three models. The paraffin oil (PO) model consisted of linear alkanes of 18 carbon atoms having a molecular formula (n-$C_{18}H_{38}$). The models of these molecules were optimized by MNDO/d semi-empirical method [Dewar et al. (1977)]. **Fig. 4.9** provides the optimized structures of these molecules. The adsorption surface was a metallic Fe (110) surface slab of dimensions (42.90Å ×42.90Å×8.58 Å). The complete system consisted of this Fe (110) slab as the XY plane and was 108.40Å long in the Z direction. One molecule of the considered pyranopyrazole derivative, along with 20 alkane molecules (PO), was placed next to the Fe (110) surface. The amorphous builder in the MAPS 4.1 platform executed this part. The conjugate gradient approximation method was applied to remove all unfavorable overlapping due to the random solvation of all molecules. The PO layer (along with the additive molecule) had an initial liquid

density and was relatively compact. As such, a large volume of the initial system (in the Z-direction after the PO layer) was empty. While periodic boundary condition was applied in all three directions, the large vacuum (empty space) in Z-direction made the system effectively non-periodic in this direction.

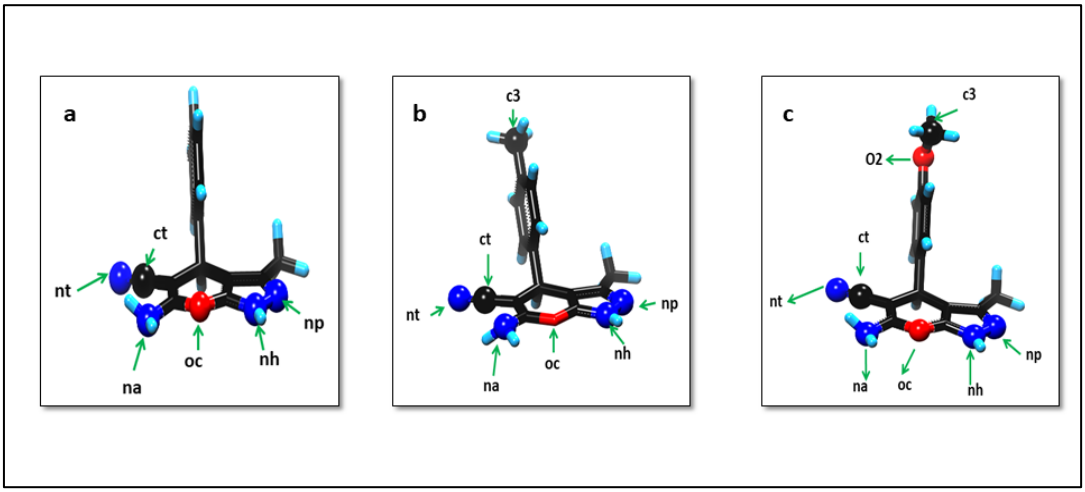

Fig. 4.9. Optimized structure by MNDO/d semiempirical method (a) PPz-H, (b) PPz-Me, and (c) PPz-OMe

Three systems were made in this manner and are henceforth denoted by PPz-HS, PPz-MeS, and PPz-OMeS (containing PPz-H, PPz-Me, and PPz-OMe additive molecules, respectively) abbreviations in this research article. The SCIPCFF (Scientific Polymer Consistent Force field) force field using the 9-6 Lennard-Jones non-bonded potential [Sun et al.(1994), Kuntail et al.(2019)] was applied to these systems. **Table 4.2** gives the Lennard-Jones parameters used in the SciPCFF force field for the atom types making up the systems. Long-range electrostatic interactions were calculated by the Particle Mesh Ewald approach with a 12 Å cutoff distance.

Table 4.2. LJ 9-6 Potential Parameters used in calculations

Atom type	r	Eps
Fe	2.6595	13.8892
nt	3.5700	0.06500
ct	4.0100	0.06400
na	4.0700	0.06500
nh	4.0700	0.13400
np	3.5700	0.04100
oc	3.3000	0.09600
c3	3.9320	0.33500
O2	3.3080	0.1200
hn	1.6500	0.01300
hc	1.0870	0.00800

The large-scale atomic/molecular massively parallel simulator (LAMMPS) program was used to run the MD simulations [Plimpton et al. (1995)] under NVT conditions for 8 nanoseconds with a time step of 1fs at 298K. The Nose-Hoover thermostat (as in the LAMMPS package) maintained the system temperature at 298K during the MD simulations. The positions of Fe atoms in the iron slab were fixed for the whole simulation. All three systems got equilibrated

within 2 nanoseconds of the MD simulation run. Thereafter, a long MD production run of 6 nanoseconds was performed to collect data for the calculation of the ensemble average potential energies of different systems and radial distribution function analysis.

4.2. Results and discussion

At first, considering concentration as the most important variable for activity, the concentration of the additives was optimized to give the best results. **Fig. 4.10** exhibits the plots of mean wear scar diameter (MWD) of steel balls as a function of concentration under the conditions of the ASTM D4172 test.

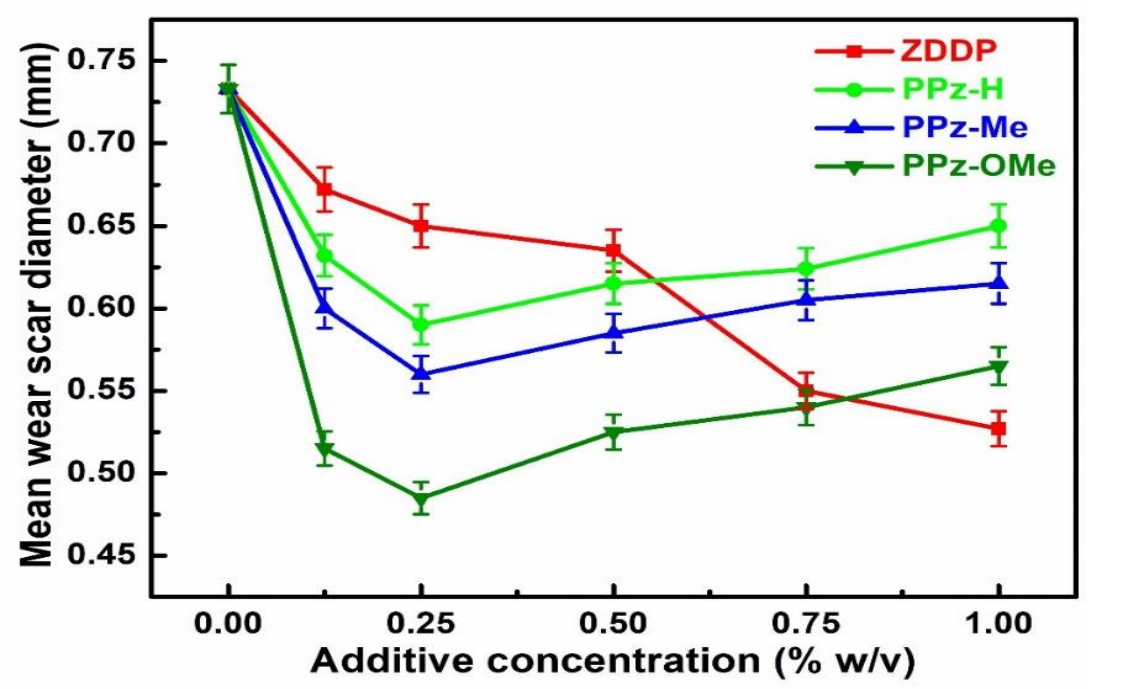

Fig. 4.10. Variation of mean wear scar diameter with the concentration of ZDDP and different pyranopyrazole additives in PO at 392 N applied load for 60 min duration

The figure itself manifests that all investigated additives are tribologically active at all the studied concentrations because the values of MWD are lowered enough in each case compared

to blank paraffin oil. At 0.125%w/v of the additives, a significant dropping in MWD starts and continues up to 0.250%w/v. In contrast, further additions of the additives raise the value of MWD. Thus, 0.250%w/v appears to be the optimized concentration for the additives when persistent tribofilm is formed. Beyond 0.250%w/v concentration, undue friction and wear are caused by an excess amount of unadsorbed additive. The standard additive ZDDP shows its best activity at 1% concentration [Kumar et al. (2019)]. Among the additives, it was observed that substituted pyranopyrazoles performed better than that the unsubstituted. The activity increases further on varying the substituents from methyl to methoxy.

Given our earlier reports [Jaiswal et al.(2014)] regarding the synergistic activity of nitrogen-containing compounds with borate ester, the tribological experiments were also performed taking the most active additive PPz-OMe and a borate ester (van lube 289) in the ratio 1:1 of the total optimized concentration.

4.2.1. Tribological studies

4.2.1.1. Wear and friction studies (ASTM D4172 Test)

Fig. 4.11 envisages the information in the form of bar diagrams regarding the variation of MWD in the presence of plain paraffin oil and its blends with different additives for the optimized concentration under ASTM D4172 conditions.

The MWD value for plain paraffin oil, 0.735 mm, undergoes almost 11, 20, 24, and 34% reduction in the presence of ZDDP, PPz-H, PPz-Me, and PPz-OMe, respectively, indicating maximum antiwear efficiency for the methoxy derivative. Further, assuming synergism between nitrogenous compounds and borate ester, antiwear properties of a 1:1 mixture of the most active additive and borate ester, PPz-OMe+BE having a total concentration of 0.25%,

have also been tested.

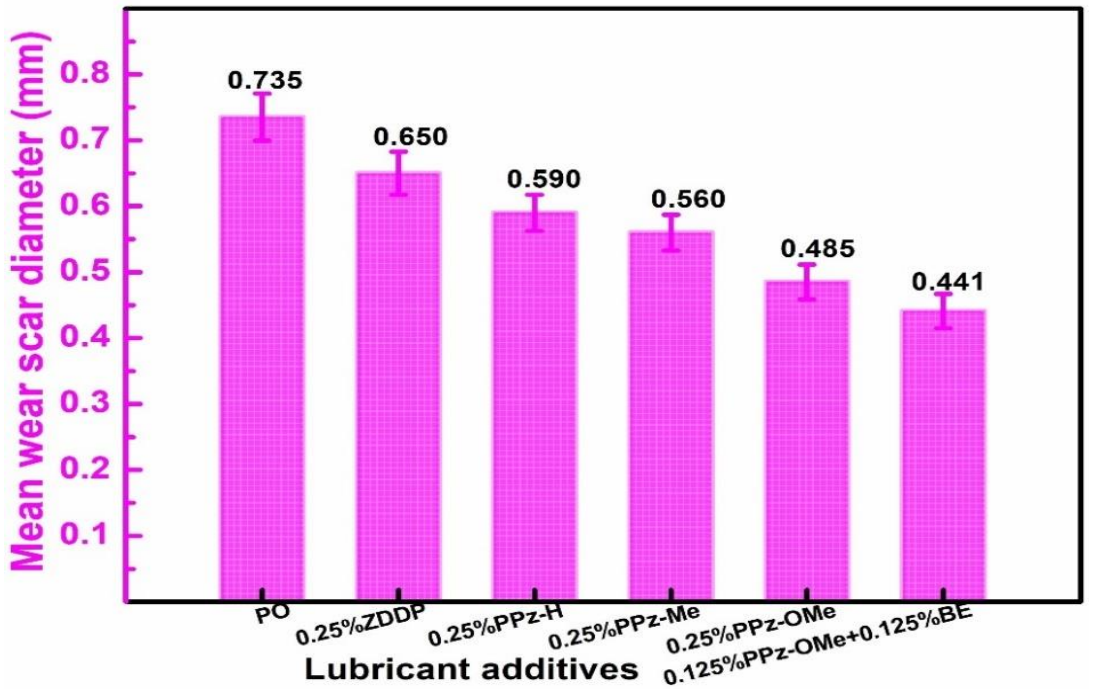

Fig. 4.11. Variation of mean wear scar diameter in the absence and the presence of ZDDP, pyranopyrazoles, and a mixture of the most active additive PPz-OMe and borate ester in PO under ASTM D 4172 conditions

The results are shown in the form of a bar diagram in **Fig. 4.11**. It is apparent from the figure that there is a substantial increase in the antiwear behavior of the mixture as the % reduction in MWD has reached around 40%. Thus, the results are indicative of the presence of synergic interaction between pyranopyrazole and borate ester. **Fig. 4.12** relates to the alteration of the coefficient of friction with time in the presence of paraffin oil alone and its blends with the synthesized additives. As anticipated, the coefficient of friction in the absence of additives is

very high throughout the test period. However, in the presence of additives, its values are remarkably reduced. The sequence of reduction is the same as discussed above. In general, for a particular blend, the coefficient of friction is unstable in the beginning as the process of adsorption has just initiated. Still, with a traverse of time, it gets considerably reduced and stabilized.

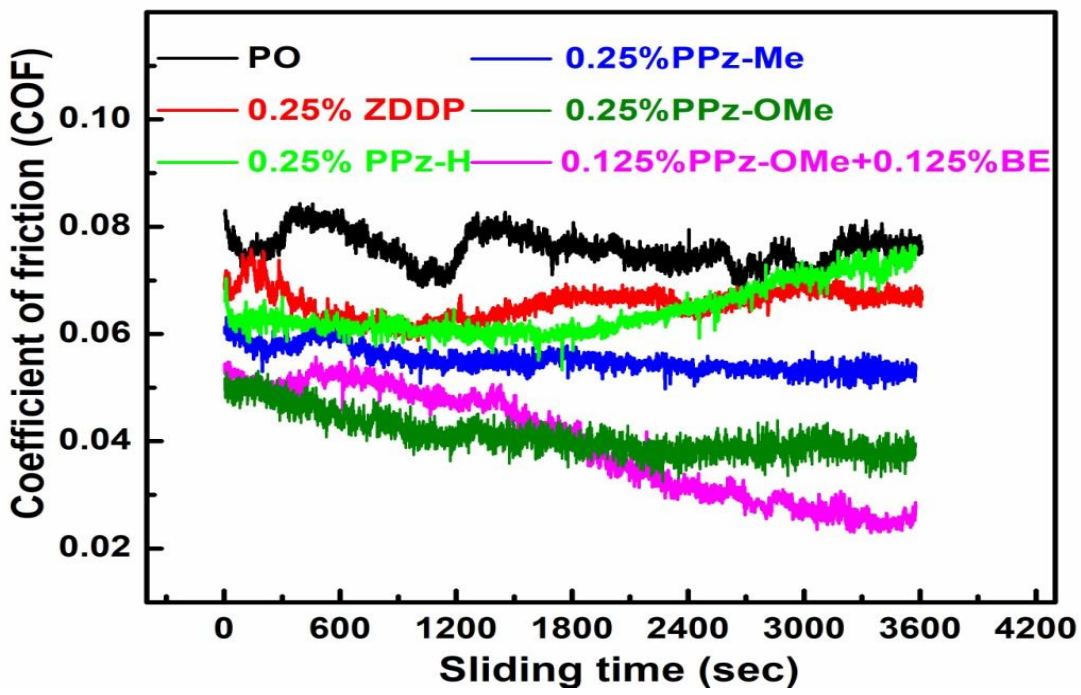

Fig. 4.12. Variation of the coefficient of friction with sliding time in the absence and thpresence of different pyranopyrazoles, ZDDP, and mixture of the most active additive PPz-OMe and borate ester in PO under ASTM D 4172 conditions

Dependence of COF on time reflects that initially, there is no tribofilm between the moving surfaces, but as time passes, additive molecules get strongly adsorbed over the proximal surfaces during sliding motion under working conditions and may interact with the metal surface to form tribofilm, causing COF values to decline. Finally, after the formation of consistent tribofilm, COF is drastically reduced. Further, the synergic interaction could be noticed between PPz-OMe and borate ester since the coefficient of friction values are reduced drastically. Variation of MWD with 0.25 to 1.5 h time at the interval of 15 min under the load of 392 N in the presence of blank base lube and its formulations with the synthesized additives has also been examined. For wear rate determination, MWD has been converted into mean wear volume (MWV).

4.2.1.2. Determination of wear rate

Wear rate has been determined by considering the linear regression model in MWV vs. time graphs (**Fig. 4.13**). Time up to 0.75 h has been contemplated as a running-in period (**Fig. 4.14**), while from 0.75-1.25 h, it is steady-state (**Fig. 4.15**). The high values of running-in and steady-state wear rate for blank base lube are significantly reduced in the case of blends obviously in tune with antiwear data (**Table 4.3**). Thus, the most significant reduction in wear rates is observed in the case of additive PPz-OMe. Its mixture with borate ester exhibits a further reduction in wear rates, therefore validating the synergy between them again.

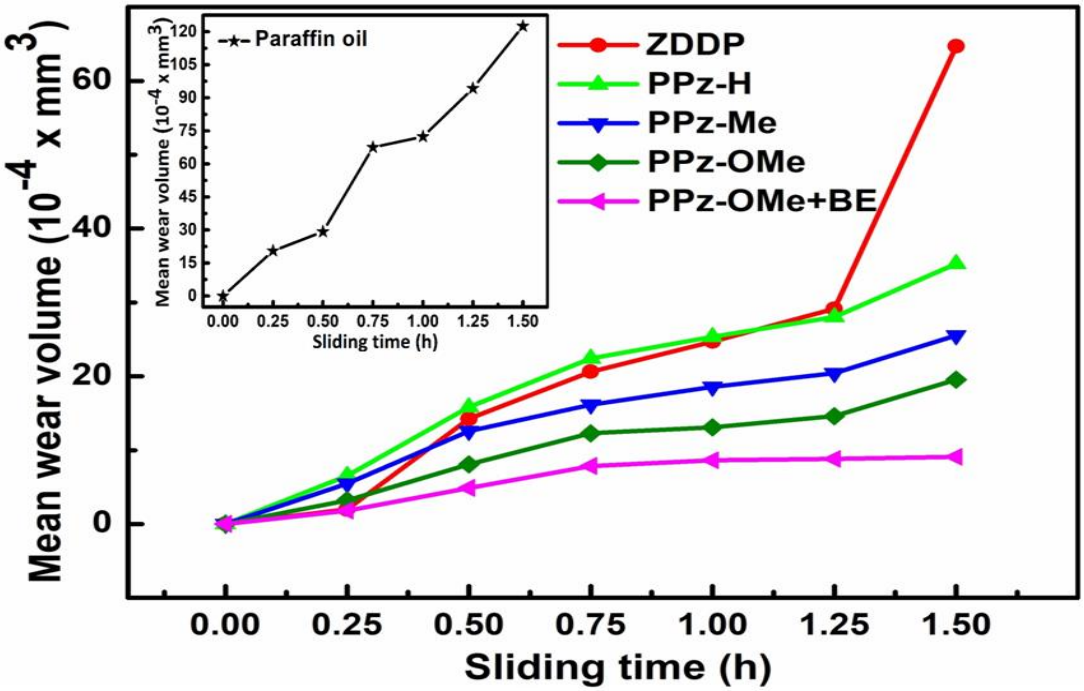

Fig. 4.13. Variation of mean wear volume with sliding time (h) for PO with or without 0.25% w/v of pyranopyrazoles, ZDDP, and 1:1 mixture of PPz-OMe and borate ester at 392N applied load.

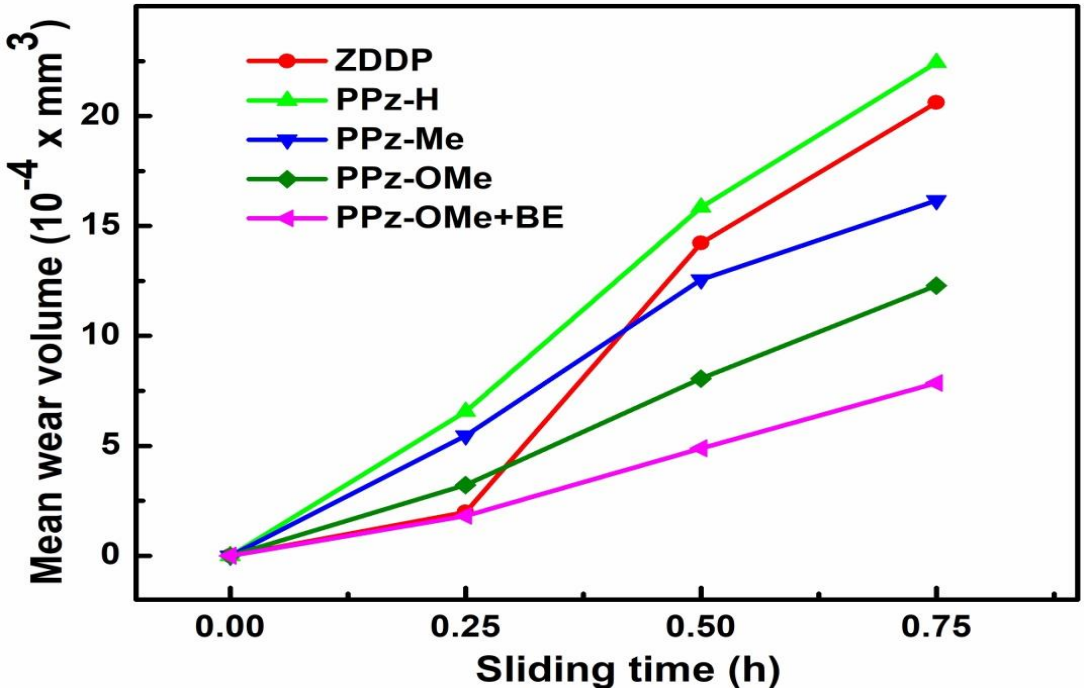

Fig. 4.14. Determination of running-in wear rate by varying mean wear volume with sliding time (h) for PO with or without 0.25% w/v of pyranopyrazoles, ZDDP, and 1:1 mixture of PPz-OMe and borate ester at 392N applied normal load

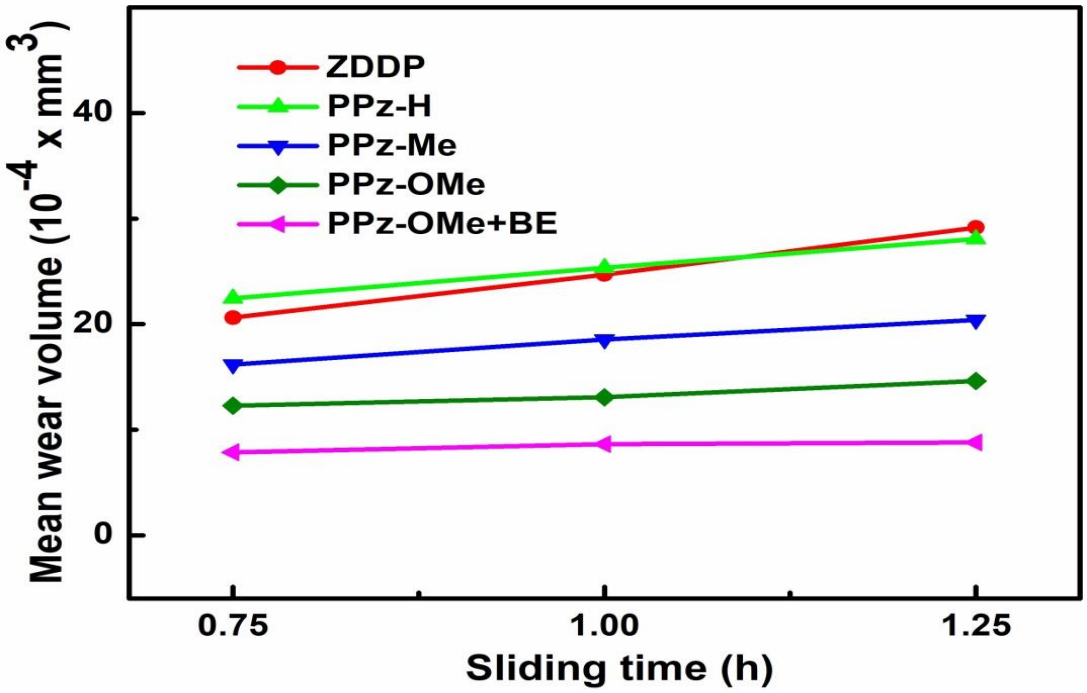

Fig. 4.15. Determination of steady-state wear rate by varying mean wear volume with sliding time (h) for PO with or without 0.25% w/v of pyranopyrazoles, ZDDP, and 1:1 mixture of PPz-OMe and borate ester at 392N applied normal load

Table 4.3. Wear-rate for PO in the presence and absence of pyranopyrazoles for 60 min test duration at 392N applied load

S.N.	Lubricants	Wear rate (10^{-4} x mm^3/h)	
		running-in	steady-state
1	PO	84.48	53.32
2	ZDDP	29.41	22.78
3	PPz-H	30.16	24.71
4	PPz-Me	22.59	17.98
5	PPz-OMe	16.06	12.98
6	PPz-OMe + BE	10.04	8.16

4.2.1.3. Compatibility of pyranopyrazoles with a borate ester

The antiwear behavior, average COF, wear rate data (shown in **Figs. 4.11, 4.12, and 4.13,** respectively), and the morphology of worn surface by SEM, AFM, and XPS illustrate strong compatibility of PPz-OMe with borate ester.

4.2.2. Characterization of worn surfaces

For analyzing the morphology of the surface of wear scar on steel ball after ASTM D4172 tribological test, surface studies by scanning electron microscopy (using ZEISS SUPRA 40) and atomic force microscopy (using Nano surf easyscan2) have been performed. SEM micrographs of the worn steel surface in the presence of base oil alone and its blends with pyranopyrazoles are shown in **Fig. 4.16**. The inset of the micrograph presents a full view of the wear scar. The size of the wear scar corroborates the order of tribological activity obtained

experimentally. Thus, the PPz-OMe derivative imparts a minimal size of wear scar. Regarding the smoothness of the tribo surface, similar order may be arguably endorsed. Accordingly, the evenest surface is observed again in the presence of blend PPz-OMe, whereas the least smooth surface with deep furrows is observed in the case of plain base lube. Furthermore, in the presence of a synergic mixture of PPz-OMe and borate ester, the wear scar is severely reduced.

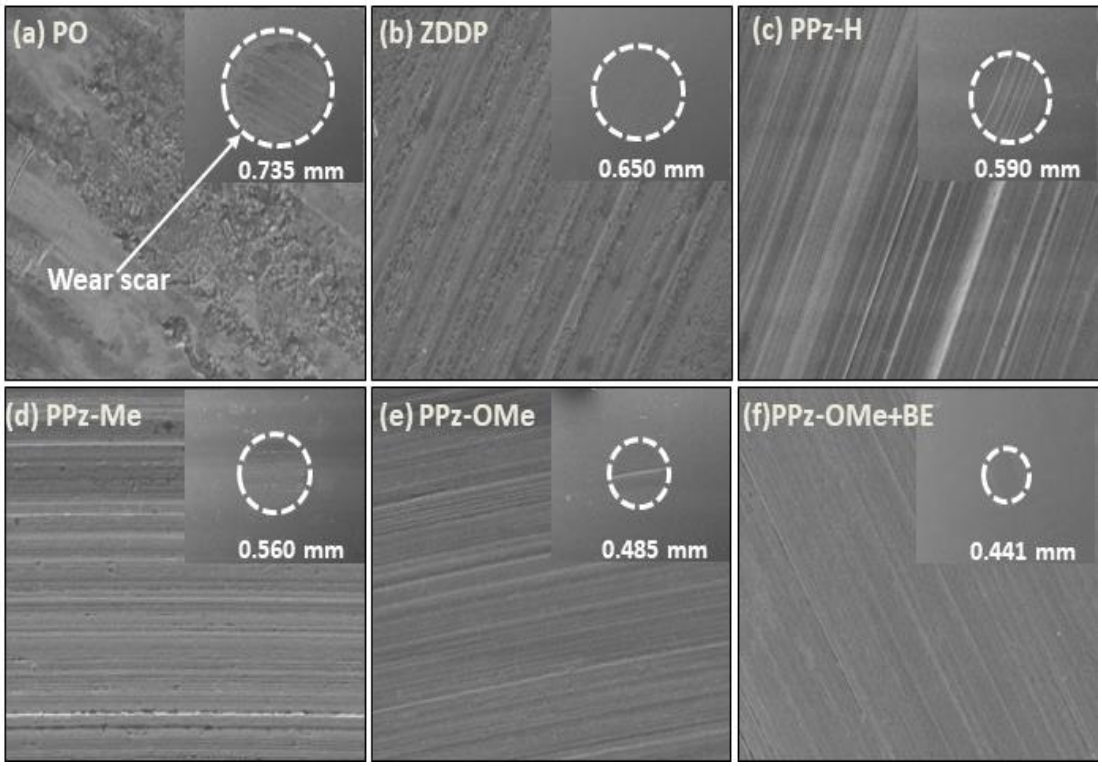

Fig. 4.16. (**a-f**) SEM images from (inset: full view of wear scar at 100X, wear scar surface at 2.00kX magnification) of the worn steel surface lubricated with PO in the presence and absence of different additives (0.25% w/v) and the mixture (0.125 % PPz-OMe + 0.125 % BE) under ASTM D4172 test conditions

The Energy Dispersive X-ray Spectroscopy (EDX) of wear scar on the steel balls lubricated with blank oil and its blends with different additives has been carried out after ASTM D4172 test to find out the elemental composition of the tribofilm. However, for the sake of brevity, these are not being shown here. The EDX spectrum for a mixture of PPz-OMe and borate ester is only shown in **Fig. 4.17(b)**. According to presumption, heteroatoms are perceived as nitrogen and oxygen. These heteroatoms are of paramount significance in the formation of a tribochemical film. The element boron could not be detected possibly, due to the small size in the EDX spectrum.

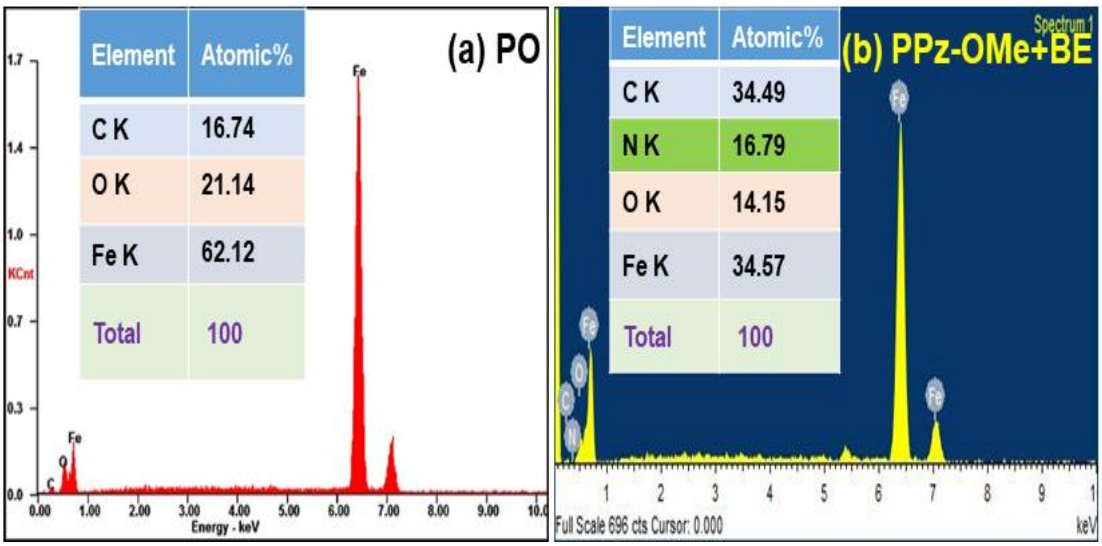

Fig. 4.17. EDX spectra of worn surface lubricated with (a) PO and (b) PPz-OMe+BE

The roughness parameters of wear scars [root mean square area (Sq) and root mean square line roughness (Rq)] were recorded for base oil, its admixtures with the reference additive, and the most triboactive additive PPz-OMe. The roughness data acquired from contact-mode AFM

studies after ASTM D4172 test are presented in **Fig. 4.18** along with their 3D AFM images.

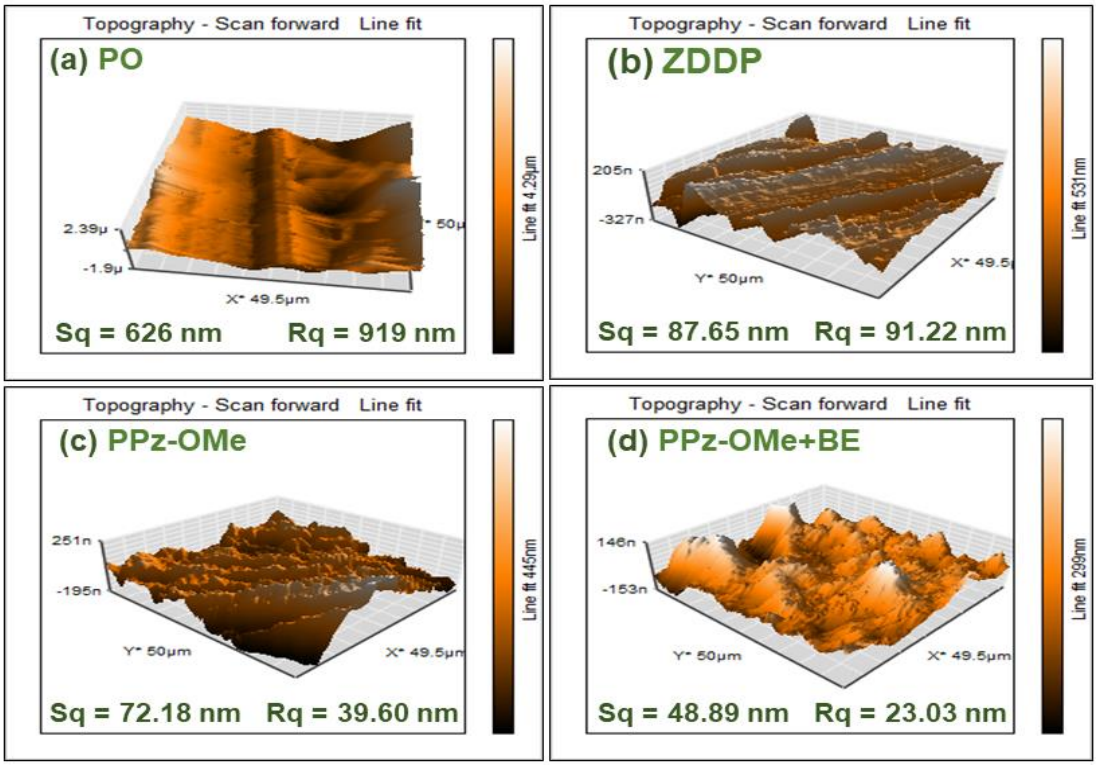

Fig. 4.18. (a-d) 3D AFM images of the worn steel surface lubricated with PO in the presence and absence of different additives (0.25% w/v) and the mixture (0.125%PPz-OMe + 0.125% BE) under ASTM D4172 test conditions

The roughness values in the presence of paraffin oil were found to be much higher (Sq= 626 nm, Rq = 919 nm). These values are reduced to 87.65 nm and 91.22 nm, respectively, in the case of the reference additive ZDDP. An enormous reduction in these values is noticed in the presence of the best additive PPz-OMe (Sq = 72.18 nm, Rq = 39.60 nm). An enormous diminution is observed in the surface roughness data (**Fig. 4.18**) for the mixture PPz-OMe and

borate ester (Sq = 48.89 nm, Rq = 23.03 nm).

The XPS study of the wear track in the presence of PPz-OMe+BE mixture is subjected to determine the chemical composition of the tribofilm formed under ASTM D4172 standards test conditions and to analyze the mechanism of the viewed synergistic interaction of PPz-OMe with borate ester in PO. The deconvoluted XPS spectra of B 1s, N 1s, C 1s, O 1s, and Fe 2p of the tribofilm using a mixture of PPz-OMe and BE after conducting ASTM D4172 test are shown in **Fig. 4.19**. The spectrum of B1s, **Fig. 4.19 (a),** reveals two peaks at 190.2 and 194.0 eV binding energies corresponding to BN, and B-O bonds, respectively [Jaiswal et al.(2014)]. The N 1s spectrum is depicted in **Fig. 4.19 (b)**. The peak present around 399.8eV confirms BN bond formation [Jaiswal et al.(2014)]. The spectrum of C1s, **Fig. 4.19 (c),** exhibits three peaks at 284.5, 285.0, and 288.1 eV corresponding to C-C/C=C, C-O/C-N, O-C=O bonds, respectively [Verma et al.(2018), Kumar et al.(2019), Sordello et al.(2014)]. **Fig. 4.19 (d)** shows the core-level spectrum of O 1s, indicating three peaks with binding energies 530.4, 531.1, and 532.4 eV corresponding to Fe-O/Fe_2O_3, C-O/O-C=O, B_2O_3 moieties respectively [Yang et al. (2011), Yang et al.(2017)]. The binding energies of Fe 2p at 710.6 eV (**Fig. 4.19 e**) and O 1s at 530.4 eV (**Fig. 4.19 d**) affirms the formation of iron oxides FeO and Fe_2O_3 due to the oxidation of steel surface iron during tribo test [Zhou et al. (2001)]. The binding energies in B 1s at 190.2 eV (**Fig. 4.19 a**) and N 1s at 399.8 eV (**Fig. 4.19 b**) together indicate the formation of boron nitride (BN) [Jaiswal et al. (2014), Yao et al. (1997), Li et al.(2014), Yan et al. (2014), Li et al.(2015), Qiao et al.(2003)]. Besides this, a weak peak at 194.0 eV in the B 1s spectrum (**Fig. 4.19 a**) relates to the formation of B_2O_3 [Jaiswal et al. (2014)]. Thus, it may be inferred that pyranopyrazole and borate ester have interacted together with the steel surface

under tribo conditions to yield BN, B_2O_3, Fe_2O_3, and boron-iron glassy network [Philippon et al. (2011)] along with decomposed additive. The constituents of the tribofilm rendered active participation in exceeding lubricating behavior.

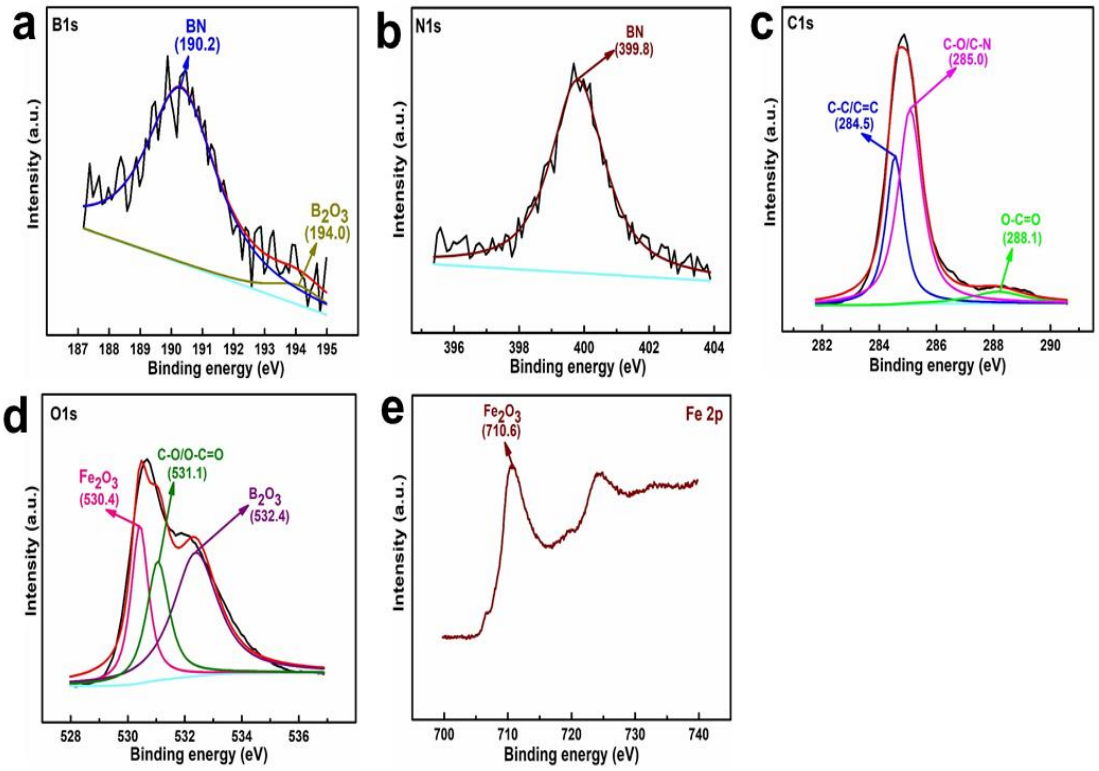

Fig. 4.19. XPS spectra of tribochemical film formed on worn steel surface lubricated with the mixture(0.125 % PPz-OMe + 0.125% BE) at 392 N applied load for 60 min test duration in PO (a) B 1s (b) N 1s (c) C 1s (d) O 1s and (e) Fe 2p

4.2.3. Tribochemistry and proposed mechanism for tribological action

As discussed above, it may be unequivocally stated that the pyranopyrazole additives behave as highly tribologically active formulations. The AFM and SEM results are in agreement with

the experimental data. EDX analysis furnishes enough evidence in favor of heteroatoms present on the tribo surface showing strong adsorption of the additives on the interacting surfaces through their heteroatoms. The tribological interaction of additives with the metal surface ends up in a strong, adherent, and persistent tribochemical film, which indeed alleviates the contacting surfaces reducing friction and wear, and finally bears the load. Furthermore, the experimental order of activity of different additives is validated by morphological studies results.

The compatibility of the best additive PPz-OMe with borate ester yielded encouraging results involving a synergistic approach. The nitrogen atoms of PPz-OMe, being electron-rich, are capable of donating electrons to the electron-deficient boron atom of borate ester-forming boron nitride, which could be validated from XPS studies of the worn surface. The *in situ* formed BN being itself an excellent lubricant with a layered structure, certainly enhances lubrication. Besides BN, B_2O_3 [Spardo et al. (2018)] also adds to lubrication. The surface Fe^{3+}, a hard Lewis acid, strongly interacts with borate ester, a hard base. Thus, Fe^{3+}enters into a glassy borate structure [Philippon et al. (2011)], and the triboactivity is increased. Theoretical studies, quantum chemical computations, and molecular dynamics simulation studies were also performed to corroborate the experimental order of tribological activity of different pyranopyrazoles.

4.3. Quantum chemical computations

Quantum chemical computation was carried out to examine the effect of substituents on the pyranopyrazoles in modifying antiwear properties.

4.3.1. Density functional theory (DFT) calculations of different additives

The structures of different pyranopyrazoles have been correlated with the practically determined wear-rates. **Fig. 4.20** exhibits full geometry optimized structures of the prepared pyranopyrazole additives PPz-OMe, PPz-Me, and PPz-H. For tribo-action, at first, the additive molecules are adsorbed physically or chemically on the tribo surfaces for further interaction. Frontier Molecular Orbital Theory (FMO) may be invoked to provide a plausible explanation for the observed friction and wear-reducing tendencies. **Table 4.4** displays computational data for quantum chemical parameters like total energy, the energy of the highest occupied molecular orbital (E_{HOMO}), the energy of lowest unoccupied molecular orbital (E_{LUMO}), and the energy difference between the HOMO and LUMO (ΔE).

The parameters E_{HOMO} and E_{LUMO} play a vital role in explaining the reactivity of the additive molecule. According to Hartree–Fock theorem [Philippon et al. (2011), Huang et al. (2003)], ionization potential (I) corresponds to ($-E_{HOMO}$), whereas electron affinity is given as ($-E_{LUMO}$). The absolute electronegativity (χ) is taken as the mean of ionization potential and electron affinity. The mean value of the difference between ionization potential and electron affinity is defined as the global hardness (γ). The inverse of global hardness is termed global softness (σ). When the additive interacts with the metal surface, electrons flow from the additive to the metal to reach equal chemical potentials.

Table 4.4. Computed quantum chemical variables for Pyranopyrazoles using B3LYP/6-31G + (d, p) basis set

Additives	Fe_5	PPz-OMe	PPz-Me	PPz-H
Total Energy (a.u.)		-949.48	-874.27	-834.95
E_{HOMO} (Hartree–Fock)	-0.18651	-0.22342	-0.23070	-0.23253
E_{LUMO} (Hartree–Fock)	-0.06420	-0.03303	-0.03507	-0.03663
ΔE (Hartree–Fock)	0.12231	0.19039	0.19563	0.19590
I	0.18651	0.22342	0.23070	0.23253
A	0.06420	0.03303	0.03507	0.03663
χ	0.12535	0.12823	0.13289	0.13458
γ	0.06115	0.09520	0.09782	0.09795
σ	16.35322	10.50420	10.22286	10.20929

The additives with the highest stability index are those which show the largest ΔE and behave as inert (hard) species during a chemical reaction. Conversely, additives with the smallest ΔE show the lowest stability index and tend to be soft or easily polarized. Correspondingly, the tribological performance may be predicted to increase from the PPz-H to PPz-OMe through PPz-Me. The order matches absolutely with the experimentally observed order for wear rates.

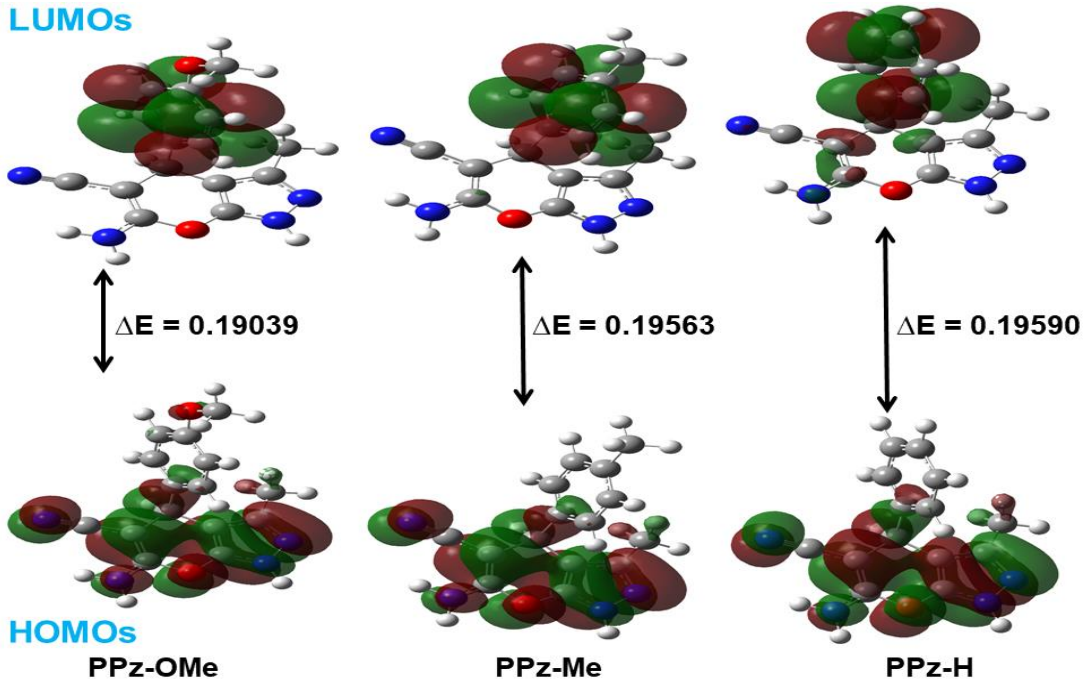

Fig. 4.20. HOMO and LUMO of pyranopyrazoles including the difference in their energy (ΔE)

The experimentally obtained values of tribological parameters for pyranopyrazoles may be accorded with their molecular structures. As evident from the structure of the pyranopyrazole moiety, it has fused pyran and pyrazole rings. It is adsorbed on the tribo surface through nitrogen atoms of the pyrazole group and oxygen of the pyran ring. The nitrogen atoms of the pyrazole ring, being delocalized with the ring, are involved in surface adsorption. Besides this, three substituents, -NH_2, -CN, and benzene ring with *p*-substitution, are also present on the pyran ring. These are also supposed to be involved in adsorption. The cyanide group being electron-withdrawing and having –I effect results in the accumulation of electron density over it, as conspicuous in the HOMO diagram **Fig. 4.20**, which should be easily associated with

adsorption. The amino group having electron density on the nitrogen atom should also be actively associated with adsorption. However, the figure shows that electron density is delocalized with the pyran ring as well as a cyanide group. Thus a delocalized system of -NH_2, cyanide, and pyran ring interacts with the metal surface. The tribological activity of different derivatives of pyranopyrazole may be interpreted on the characteristics of various substituents placed at the *p*- position of the benzene ring. Thus, the tribological performance of PPz-OMe is the greatest, PPz-H is the least, while PPz-Me stands in between the two. The observed trend may be associated with the electron density on the benzene ring attached to the *p*- position of the pyran ring. The better electron-donating tendency of the methoxy group than that of the methyl group yields better results for the former than the latter. The compatibility of pyranopyrazole with borate ester may be explained by invoking the coordination tendency between nitrogen with lone pair of electrons and boron having insufficient electrons.

4.3.2. Molecular Dynamics Simulations (MD)

4.3.2.1. Adsorption Energy Calculation

The potential energy of adsorption, E_{ads} , between the iron surface and the pyranopyrazole derivative was calculated as follows:

$$\mathbf{E_{ads} = E_{total} - (E_{surface} + E_{solvent} + E_{PYZ})}$$

Here E_{total} is the potential energy of the combined system of iron crystal together with the adsorbed pyranopyrazole molecule and solvent molecules. The other terms, $E_{surface,}$ $E_{solvent}$, and $E_{PYZ,}$ depict the individual potential energies of the iron slab, the solvent, and the free pyranopyrazole molecule, respectively. The adsorption energy order was found to increase in the order PPz-OMe > PPz-Me > PPz-H **(Table 4.5).** The more negative energy of PPz-OMe

indicates that it adsorbs more strongly to the iron surface.

Table 4.5. Computed adsorption energies (E_{ads}) for different pyranopyrazole derivatives

Compound	**E_{total} (kcal/mol)**	**$E_{surface} + E_{solvent} + E_{PYZ}$ (kcal/mol)**	**E_{ads} (kcal/mol)**
PPz-OMe	313033	313700	-667
PPz-Me	313087	313685	-598
PPz-H	313101	313676	-575

The wear results of these additive molecules also follow the same order. Thus, the PPz-OMe molecule gives the best anti-wear performance among the three additives considered. Next is PPz-Me, and the least active additive is PPz-H. Therefore, the relative anti-wear performances of these additive molecules can be attributed to the nature of their adsorption on the Fe surface.

4.3.2.2. Radial Distribution Functions (RDF) Analysis:

Long-time average RDF plots for interactions between different atoms of pyranopyrazole derivatives and iron atoms give a quantitative understanding of the adsorption mechanism.

Table 4.6. Atom types notations used for pyranopyrazole derivatives in RDF plot

Atom types	Description
Fe	Iron atom
Nt	The nitrogen atom of the nitrile group attached to the pyran ring
Ct	The carbon atom of the nitrile group attached to the pyran ring
Na	The nitrogen atom of the NH_2 group attached to a pyran ring
Nh	The nitrogen atom attached to a hydrogen atom in the pyrazole ring
Np	Nitrogen atom attached with a carbon atom in pyrazole ring
Oc	The oxygen atom in the pyran ring
c3	The carbon atom of the methyl group placed at the *p*- position of the benzene ring (attached to the *p*- position of the pyran ring) in PPz-Me/PPz-OMe.
O2	The oxygen atom present in the methoxy group placed at the *p*- position of the benzene ring (attached to *p*- position of the pyran ring) in PPz-OMe

Fig. 4.21a shows a typical production run snapshot of a PPz-H molecule adsorbed on the iron slab. The figure shows that the pyran and the pyrazole rings in PPz-H interact strongly with the iron atom. **Fig.4. 21b** contains the RDF plots of the corresponding atom type pairs (between Fe atoms from the slab and various atom types in the PPz-H molecule). The atom types notations used in RDF plots **(Figs. 4.21b, 4.22b, 4.23b)** are described in **Table 4.6**.

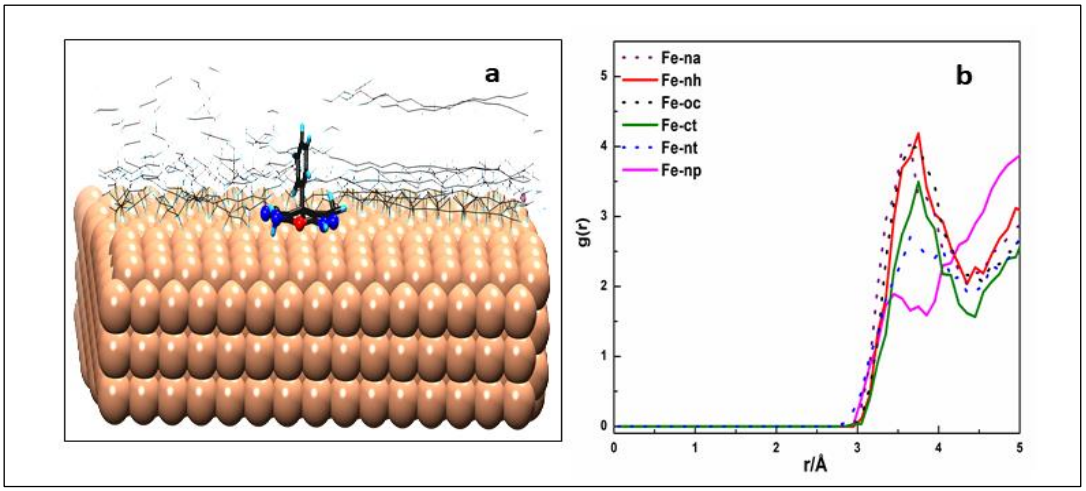

Fig. 4.21. (a) Snapshot of a typical production run conformation of PPz-H molecule adsorbed on the Fe (110) surface in the presence of PO and (b) RDF plots of different atom types in the PPz-H compound with Fe atoms.

The first peak in each RDF plot describes the nearest distance at which the two atom types are most likely to be found. Thus, the RDFs of the atom-type pairs, which have their first peak at the shortest distances (relative to other atom-type pairs), depict the strongest interactions. **Fig. 4.21(b)** shows that the RDF plots of Fe-na, Fe-nh, and Fe-oc pairs display their first peaks at approximate 3.5Å. Note that these are also the most intense peaks in this figure. The Fe-nt first peak also lies at the same distance, although it is less intense. The Fe-ct pair has its first peak at ~ 3.6Å. It is also less intense than the peaks of the other interactions mentioned above. Clearly, the PPz-H molecule interacts with the Fe surface through these atom types in the pyran and pyrazole rings of this molecule. This result matches the picture of the PPz-H molecule sitting on the Fe (110) surface using its pyran and pyrazole rings.

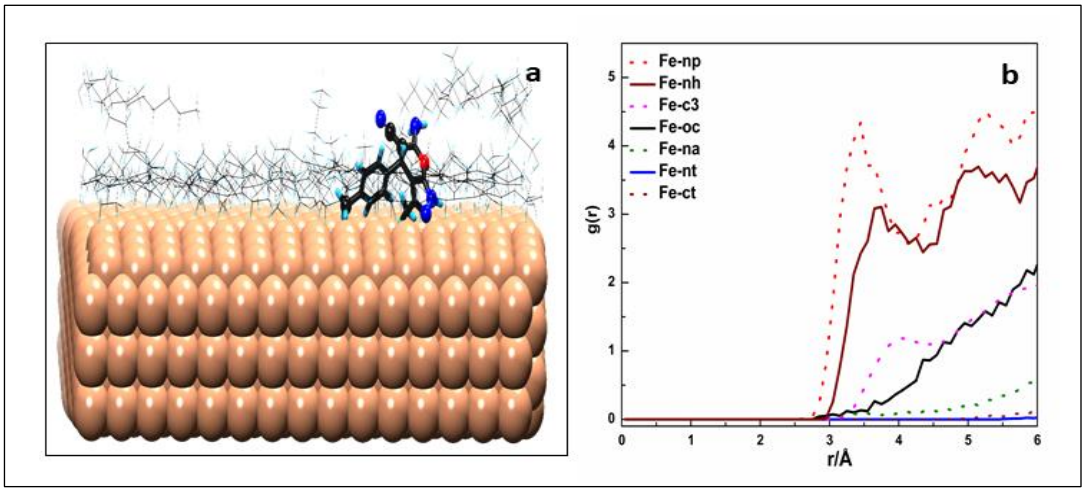

Fig. 4.22. (a) Snapshot of Equilibrium conformation of PPz-Me adsorbed molecule on the iron surface in the presence of PO and (b) Radial distribution function of a different atom of the PPz-Me compound with an iron atom at distance r

Fig. 4.22(a) displays a characteristic production run conformation of the system containing the PPz-Me molecule. It seems that the PPz-Me molecule gets adsorbed on the iron surface in the presence of PO through the pyrazole ring, and the carbon atom of the methyl group placed at the *p*- position of the benzene ring (attached to *p*- position of the pyran ring). **Fig. 4.22(b)** gives the RDFs of the interactions possible between Fe atoms of the slab and the atoms making the PPz-Me molecule. The first peak of the Fe-np RDF occurs at the shortest distance (3.4Å) in this figure. It also has the highest g(r) value among all plots. The Fe-nh pair gives the next interaction. Its first peak appears at ~ 3.6Å. The Fe-c3 (interaction between Fe and the carbon atom of the methyl group placed at the *p*- position of the benzene ring) RDF first peak is at ~ 4Å. The first peaks of the rest of the possible atom pairs occur at longer distances. Therefore, the PPz-Me molecule adsorbs to the Fe atoms on the (110) surface through the two nitrogen

atoms of the pyrazole ring [Fe-np and Fe-nh] and the methyl carbon located at the *p*-position of the benzene ring (attached to *p*-position of pyran ring) in PPz-Me [Fe-c3]. This quantitative description is consistent with the picture of the production run conformation of this system (**Fig. 4.22a**).

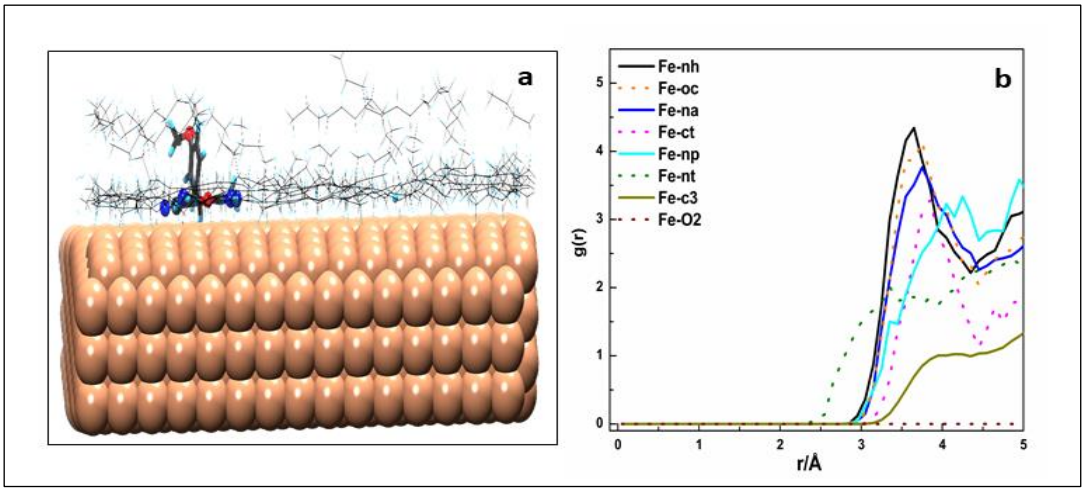

Fig. 4.23. (a) A production run conformation of PPz-OMe adsorbed molecule on the iron surface in the presence of PO and (b) RDF plots of different atoms of the PPz-OMe compound with Fe atoms in the iron slab

Fig. 4.23a shows that the PPz-OMe molecule appears to sit on its pyran and pyrazole rings. In other words, the planes of these rings look nearly parallel to Fe (110) surface. The first peaks of the RDF plots of Fe-nh, Fe-oc, and Fe-na pairs occur around ~3.5Å **(Fig. 4.23b**). These are also the strongest RDF peaks in this figure. The Fe-nt RDF peak comes earlier at ~3.3Å, but it is less than the others mentioned earlier. One can conclude that nitrogen and oxygen in the pyran and pyrazole rings are almost equally associated with Fe atoms in this system. The same

is also apparent from the picture in part (a) of this figure.

4.4. Conclusions

Being potential friction and wear modifiers, the tribological properties of environmentally benign substituted pyranopyrazoles (having a fused heterocyclic ring system) were investigated in this research. A multicomponent synthetic pathway was adopted for their preparation. Spectroscopic analysis by FT-IR and NMR (^{1}H and ^{13}C) revealed the successful preparation of H-, methyl-, and methoxy- group substituted pyranopyrazole molecules. All three pyranopyrazoles exhibited their maximum tribological activities at only 0.25%w/v concentration. The ASTM D4172 tribological tests and wear rates showed that the activities of these pyranopyrazole derivatives followed the ZDDP < PPz-H < PPz-Me < PPz-OMe ascending order. The wear scar surface analysis by SEM and AFM revealed features in consonance with tribological activity order. The presence of heteroatoms nitrogen and oxygen along with carbon on the steel surface validated the adsorption of the additives on the wear surface. DFT calculations show that PPz-OMe is relatively easy to polarize and interacts more strongly with the wear surface. The adsorption energies found from the MD studies followed the same trend as those from the DFT calculations. The additive PPz-OMe has the most negative adsorption energy and thus interacts most strongly with the adsorbent surface. The mechanism of interaction between the additive molecules with the wear surface was understood through RDF analysis enabled by MD simulation results. The RDF plots show that nitrogen and oxygen in the pyran and pyrazole rings of PPz-OMe are almost equally associated with Fe atoms. In contrast, the additive PPz-Me interacts with the adsorbent mainly through the two nitrogen atoms of the pyrazole ring and the methyl carbon attached to the benzene ring

(present at the *p*- position of the pyran ring. Thus, the optimum interaction of heteroatoms of the additive molecule with the wear surface is necessary for obtaining the best possible tribo-activities.

In addition to the above, mixing borate ester with PPz-OMe enhanced the tribological activity compared to that observed for pure additive. XPS studies of the surface after the ASTM D4172 test showed the formation of boron nitride. It seems the latter is responsible for the synergistic increase in tribological activity.